Available online at www.sciencedirect.com
ScienceDirect
International Journal of Thermal Sciences 47 (2008) 209–220
International Journal of Thermal Sciences
www.elsevier.com/locate/ijts

A non-iterative pressure based scheme for the computation of reacting radiating flows

A. Bilge Uygur [a], Nevin Selçuk [a,*], I. Hakki Tuncer [b]

[a] *Department of Chemical Engineering, Middle East Technical University, 06531 Ankara, Turkey*
[b] *Department of Aerospace Engineering, Middle East Technical University, 06531 Ankara, Turkey*

Received 8 October 2006; received in revised form 21 February 2007; accepted 21 February 2007

Available online 12 April 2007

Abstract

A non-iterative pressure based algorithm which consists of splitting the solution of momentum energy and species equations into a sequence of predictor–corrector stages was developed for the simulation of transient reacting radiating flows. A semi-discrete approach called the Method of Lines (MOL) which enables implicit time-integration at all splitting stages was used for the solution of conservation equations. The solution of elliptic pressure equation for the determination of the pressure field was performed by a multi-grid (MUDPACK package) solver. Radiation calculations were carried out by coupling an existing radiation code to the algorithm. A first order Arrhenius type rate law expression was utilized to account for the chemistry. The predictions of the algorithm were benchmarked against experimental and numerical data available in the literature. Overall comparisons reveal that numerical results obtained with and without radiation mimic the experimental trends closely. As expected, incorporation of radiation in the simulations leads to better agreement between the predicted and measured velocity and temperature fields when compared to that obtained without radiation. The algorithm developed is an accurate and efficient tool for the simulation of reacting radiating flows and its extension to turbulent flows with the improvement of the existing models is highly promising.

Keywords: Non-iterative schemes; Pressure based methods; Operator-splitting; Reacting radiating flows; MUDPACK; Method of Lines (MOL)

1. Introduction

Numerical simulation of unsteady reacting flows such as diffusion or premixed flames are characterized by the very different time and space scales controlling physical and chemical processes. The physical and chemical processes can cover time scales ranging over nine orders of magnitude and space scales ranging over five orders of magnitude [1]. Moreover, incorporation of detailed reaction mechanisms and radiation models with varying complexity in the simulation of these flows results in a large number of equations to be solved in conjunction with the other conservation equations and hence in excessive computation times. Considering today's limited computer resources together with the difficulties listed above, a significant amount of research effort has focused on the development of efficient algorithms which will enable the investigation of flame structure and dynamics.

In view of this, a novel CFD code based on Method of Lines (MOL) was developed in Middle East Technical University Chemical Engineering Department, for the unsteady simulation of 2D incompressible, separated, internal, non-isothermal flows in regular and complex geometries [2]. The code uses MOL, which is an efficient semi-discrete approach for the solution of time-dependent partial differential equations (PDEs), in conjunction with (i) a higher-order spatial discretization scheme which chooses biased-upwind or biased-downwind schemes in a zone of dependence manner; (ii) a parabolic algorithm for the computation of axial pressure gradient which does not require the solution of an elliptic equation for pressure; (iii) an elliptic grid generator using body-fitted coordinate system for application to complex geometries. The validity and the predictive ability of the code were tested by applying it to the simulation of laminar/turbulent, isothermal/non-isothermal incompressible flows and comparing its predictions with either

* Corresponding author.
E-mail address: selcuk@metu.edu.tr (N. Selçuk).

1290-0729/$ – see front matter
doi:10.1016/j.ijthermalsci.2007.02.009

Nomenclature

$\hat{C}_p$	specific heat capacity
D	diffusion coefficient
g	gravitational acceleration
$\hat{H}$	enthalpy
I	radiative intensity
j	mass flux
N	number of species
p	pressure
q	heat flux
r	radial distance
t	time
T	temperature
u	axial component of the velocity
v	radial component of the velocity
$\mathbf{v}$	velocity vector
Y	species mass fraction
z	axial distance

Greek letters

λ	thermal conductivity
μ	viscosity
ρ	density
$\dot{\omega}$	rate of reaction

Subscripts

A	air
F	fuel
k	species
km	mixture-averaged
ref	reference

Superscripts

n	present time level
$*$	first-intermediate level
$**$	second-intermediate level
t	transpose

measured data or numerical simulations available in the literature [3,4]. In successive studies by the same group [5,6], the code was further developed by incorporation of; the solution of species equations using finite rate chemistry model together with a Total Variation Diminishing (TVD) flux limiter based discretization scheme for the computation of convective derivatives [5]; a radiation submodel to account for radiative heat transfer [6], for the simulation of transient reacting radiating flows. The predictive performance of the code was tested by applying it to the simulation of a confined laminar methane/air diffusion flame and comparing its predictions with numerical and experimental data available in the literature [7,8]. The velocity, temperature and major species concentrations obtained with and without radiation model were found to be in reasonably good agreement with numerical results and measurements [6].

Although providing a useful basis for the simulation of reacting flows, the code used in [5,6] is limited to incompressible flows due to the parabolic pressure scheme [9] embedded in the flow solver. The parabolic scheme only allows z-component of momentum equation to be solved and r-component of velocity is calculated by direct utilization of continuity equation by dropping the time derivative of density, an approach which can only be valid if the flow field is treated as incompressible. Considering the vast density changes due to temperature and concentration variations, more accurate representation of typical flows necessitates pressure based schemes which can handle all flow regimes ranging from incompressible to compressible.

Pressure based schemes in which pressure is treated as the main dependent variable and density is computed via an equation of state, have proved to be accurate and efficient in the simulation of a wide range of flows involving chemical reaction and density change [10]. Popular examples of pressure based schemes are SIMPLE by Patankar and Spalding [11] and PISO by Issa [12]. Both methods rely on the solution of an elliptic equation for pressure (either in terms of a pressure correction variable or the pressure itself) and they operate on staggered grid topology. What differs PISO from SIMPLE is that, PISO exploits the concept of operator splitting by extending it to the solution of conservation equations and offers a solution consisting of a series of implicit predictor and explicit corrector stages (splitting phases), hence it is non-iterative in contrast to the iterative SIMPLE scheme. The non-iterative nature of PISO makes it suitable for unsteady simulations whereas SIMPLE is mostly used in steady computations.

The present study focuses on the development of a PISO based algorithm for the transient simulation of reacting radiating flows and evaluating its predictive performance on the methane/air diffusion flame problem previously studied by [5–8]. Similar to PISO approach developed for reacting flows [13], the new algorithm is based on a sequence of predictor and corrector stages for momentum, energy and species equations. A pressure equation which replaces the role of equation of continuity is derived and solved at momentum corrector stages for the determination of pressure field. The differences between the proposed algorithm and PISO lie in the time-integration method and the grid topology utilized. In the present approach, the conservation equations are cast in their semi-discrete form using finite difference approximations on non-staggered grid topology which results in a system of ODEs. The resulting ODEs are integrated in time using higher-order, implicit algorithms embedded in the sophisticated ODE solvers. By this way, the present algorithm not only offers implicit hence stable time-integration at all splitting phases without extra complexity in the formulation, but also the flexibility and modularity to incorporate any desired package with ease. Moreover, with the utilization of non-staggered grid topology, easier bookkeeping is maintained throughout the algorithm as opposed to

staggered one and the feasibility of its application to complex geometries is greatly enhanced.

This paper is organized as follows: First the governing conservation equations followed by the description of the scheme are presented. The details regarding to the elements of the numerical solution technique are described next. Finally, the validation case, the numerical results obtained and the accompanying discussions are presented.

2. Governing equations

The governing conservation equations in vector notation for reacting radiating flows can be expressed as follows:

- *Continuity equation*:

$$\frac{\partial \rho}{\partial t} = -(\nabla \cdot \rho \mathbf{v}) \tag{1}$$

- *Momentum equation*:

$$\frac{\partial}{\partial t}(\rho \mathbf{v}) = -[\nabla \cdot \rho \mathbf{v}\mathbf{v}] - \nabla p - [\nabla \cdot \boldsymbol{\tau}] + \rho g \tag{2}$$

- *Energy equation*:

$$\frac{\partial}{\partial t}(\rho T) = -(\nabla \cdot \rho \mathbf{v} T) + \frac{1}{\hat{C}_p}\nabla \cdot (\lambda \nabla T) - \frac{1}{\hat{C}_p}\sum_{k=1}^{N} \mathbf{j}_k \cdot \hat{C}_{p,k} \nabla T - \frac{1}{\hat{C}_p}\sum_{k=1}^{N} \hat{H}_k \dot{\omega}_k - \frac{1}{\hat{C}_p}\nabla \cdot \mathbf{q_R} \tag{3}$$

- *Species equation*:

$$\frac{\partial}{\partial t}(\rho Y_k) = -(\nabla \cdot \rho \mathbf{v} Y_k) - (\nabla \cdot \mathbf{j}_k) + \dot{\omega}_k, \quad k = 1, \ldots, N \tag{4}$$

The pressure and density are related by an equation of state which may be represented by

$$\rho = p\psi(p, T) \tag{5}$$

Stress tensor $\boldsymbol{\tau}$ appearing in Eq. (2) is expressed using Newtonian type constitutive law of the form:

$$\boldsymbol{\tau} = -\mu\left(\nabla \mathbf{v} + (\nabla \mathbf{v})^{\mathbf{t}}\right) + \frac{2}{3}\mu(\nabla \cdot \mathbf{v}) \tag{6}$$

$\nabla \cdot \mathbf{q_R}$ is the radiative source term which can be computed by the following formula

$$\nabla \cdot \mathbf{q_R} = \kappa\left(4\sigma T^4 - \sum_m \sum_l w_{m,l} I^{m,l}\right) \tag{7}$$

once the radiative intensities (I) are calculated by the solution of Radiative Transfer Equation (RTE).

Mass flux vector $\mathbf{j}_k$ is related to species gradients by a Fickian type expression of the form

$$\mathbf{j}_k = -\rho D_{km} \nabla Y_k \tag{8}$$

The mixture-averaged diffusion formula does not have the property that the sum of the diffusive fluxes is zero, i.e, the condition,

$$\sum_{k=1}^{N} \mathbf{j}_k = 0 \tag{9}$$

Therefore, a correction is necessary to ensure mass conservation. For this purpose, rather than solving the species equation for the excess species, its mass fraction is computed simply by

$$Y_N = 1 - \sum_{k=1}^{N-1} Y_k \tag{10}$$

The diffusive flux of excess species is computed by the following formula to ensure the mass conservation constraint (Eq. (9)):

$$\mathbf{j}_N = -\sum_{k=1}^{N-1} \mathbf{j}_k \tag{11}$$

The rate of fuel consumption $\dot{\omega}_{CH_4}$ for the methane–air reaction considered in the present study is expressed using a one-step global mechanism given by Khalil et al. [14]:

$$\dot{\omega}_{CH_4} = \rho^2 Y_{CH_4} Y_{O_2} A \exp(-E_a/RT) \tag{12}$$

where $A = 10^{10}$ m^3/kg s and $E_a/R = 1.84 \times 10^4$ K.

3. Methodology

In what follows, splitting procedure for reacting radiating flows using semi-discrete formulation of the governing equations will be presented.

3.1. Semi-discrete approach

In this study, the governing equations are solved using the numerical Method of Lines which a is semi-discrete technique for the solution of time-dependent partial differential equations (PDEs). The MOL consists of two stages. First, the dependent variables are kept continuous in time and the PDEs are discretized in space on a dimension by dimension basis using any readily available spatial discretization packages such as finite-difference, finite-element or finite-volume based schemes which leads to a set of ordinary differential equations (ODEs). Next the ODEs are integrated in time using any readily available explicit or implicit ODE solver which constitutes the second step. In consideration of the MOL solution, the governing equations will be presented in their semi-discrete form for sections to come. Integration of the semi-discrete equations using an implicit ODE solver will be explained in Section 4.

3.2. Splitting procedure for reacting radiating flows

A three stage scheme in which there are one predictor and two corrector stages for momentum, energy and species will be presented (Fig. 1).

In the course of splitting; temperature, pressure and concentration dependent physical properties are updated at the start

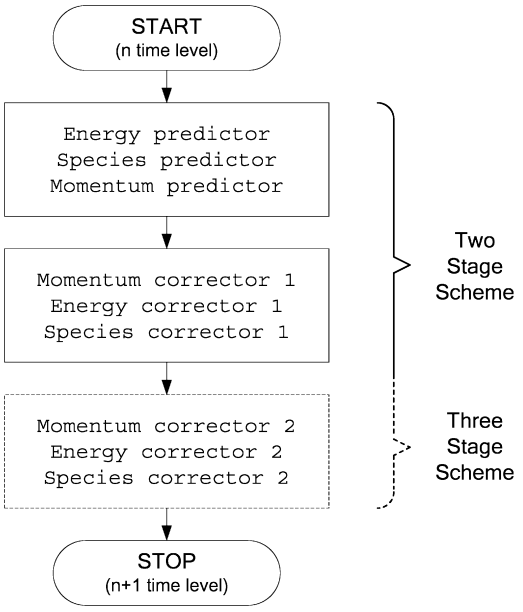

Fig. 1. Overview of the splitting procedure for reacting radiating flows.

of every stage using CHEMKIN-III [17] and TRANSPORT [18] packages; radiative source term to be used in the energy equation is computed before each energy stage by the help of radiation module.

Following the semi-discrete approach, the conservation equations at each splitting phase can be shown as

$$\frac{\mathrm{d}}{\mathrm{d}t}(\rho\phi_i) \approx Residual_i \tag{13}$$

where in this case ϕ_i is one of the dependent variables $\mathbf{v}$, T or Y_K and $Residual_i$ is finite difference representation of the terms on the right-hand side of the parent equations (Eqs. (2)–(4)). According to this notion, the residual expressions for momentum, energy and species equations are;

$$Residual_m = FD\big\{-[\nabla\cdot\rho\mathbf{v}\mathbf{v}] - \nabla p - [\nabla\cdot\boldsymbol{\tau}] + \rho g\big\} \tag{14}$$

$$\begin{aligned} Residual_e = FD\Bigg\{ & -(\nabla\cdot\rho\mathbf{v}T) + \frac{1}{\hat{C}_p}\nabla\cdot(\lambda\nabla T) \\ & - \frac{1}{\hat{C}_p}\sum_{k=1}^{N}\mathbf{j}_k\cdot\hat{C}_{p,k}\nabla T \\ & - \frac{1}{\hat{C}_p}\sum_{k=1}^{N}\hat{H}_k\dot{\omega}_k - \frac{1}{\hat{C}_p}\nabla\cdot\mathbf{q}_\mathbf{R}\Bigg\} \end{aligned} \tag{15}$$

$$Residual_{s,k} = FD\big\{-(\nabla\cdot\rho\mathbf{v}Y_k) - (\nabla\cdot\mathbf{j}_k) + \dot{\omega}_k\big\}$$
$$k = 1,\ldots,N \tag{16}$$

where the subscripts m, e and s denote that the residual expression belongs to the momentum, energy and species equations, respectively and $FD\{\}$ is a symbolic operator which simply represents the finite difference expressions in a compact form. Let the superscript n denote present time level and *, **, *** denote the intermediate values between the n and $n+1$ levels, the splitting procedure is demonstrated below.

3.2.1. Predictor stage

In order to account for the rapid variations in temperature and concentration over a time-step due to combustion, the sequence of solution commences with the energy equation then followed by species and momentum equations as suggested by [13]. The equations to be solved for this stage are:

(i) Energy predictor:

$$\frac{\mathrm{d}}{\mathrm{d}t}(\rho T) \approx Residual_e^n \tag{17}$$

(ii) Species predictor:

$$\frac{\mathrm{d}}{\mathrm{d}t}(\rho Y_k) \approx Residual_{s,k}^n, \quad k = 1,\ldots,N \tag{18}$$

(iii) Momentum predictor:

$$\frac{\mathrm{d}}{\mathrm{d}t}(\rho\mathbf{v}) \approx Residual_m^n \tag{19}$$

The solution of Eqs. (17)–(19) yields the first intermediate fields T^*, Y_k^* and $\mathbf{v}^*$. It should be noted that velocity field obtained as a result of the predictor stage does not necessarily satisfy equation of continuity since it has been obtained using a guessed (initial) pressure field.

3.2.2. First corrector stage

(i) Momentum corrector: A new velocity field $\mathbf{v}^{**}$ together with its corresponding pressure field p^* are now sought which will satisfy the discrete form of the equation of continuity for this stage

$$\frac{\rho^* - \rho^n}{\Delta t} \approx -(\nabla\cdot\rho^*\mathbf{v}^{**}) \tag{20}$$

For this purpose, a pressure equation is derived by taking the divergence of momentum equation (Eq. (2)) as follows:

$$\nabla\cdot\nabla p^* = Residual_p^* \tag{21}$$

where

$$\begin{aligned} Residual_p^* = & -\frac{\partial}{\partial t}(\nabla\cdot\rho\mathbf{v}) - \nabla\cdot[\nabla\cdot\rho^n\mathbf{v}^*\mathbf{v}^*] \\ & - \nabla\cdot[\nabla\cdot\boldsymbol{\tau}^*] + \nabla\cdot\rho^n g \end{aligned} \tag{22}$$

Using first order differences for the evaluation of time derivative of $\nabla\cdot\rho\mathbf{v}$, one obtains

$$\begin{aligned} Residual_p^* = & -\frac{1}{\Delta t}\big[(\nabla\cdot\rho^*\mathbf{v}^{**}) - (\nabla\cdot\rho^n\mathbf{v}^*)\big] \\ & - \nabla\cdot[\nabla\cdot\rho^n\mathbf{v}^*\mathbf{v}^*] - \nabla\cdot[\nabla\cdot\boldsymbol{\tau}^*] + \nabla\cdot\rho^n g \end{aligned} \tag{23}$$

The $(\nabla\cdot\rho^*\mathbf{v}^{**})$ term in Eq. (23) can be eliminated in favor of p^* by joint utilization of Eq. (20) and equation of state for this stage having the form (see Section 4 for details)

$$\rho^* = p^*\psi(p^*, T^*) \tag{24}$$

Once the corrected pressure field (p^*) is obtained by the solution of Eq. (21), ρ^* is computed by invoking Eq. (24).

Having obtained p^* and ρ^*, momentum equation for this stage

$$\frac{\mathrm{d}}{\mathrm{d}t}(\rho \mathbf{v}) \approx Residual_m^* \tag{25}$$

is solved to yield the first corrected velocity field $\mathbf{v}^{**}$.

(ii) Energy corrector: Energy equation for this stage is

$$\frac{\mathrm{d}}{\mathrm{d}t}(\rho T) \approx Residual_e^* \tag{26}$$

solution of which results in the second intermediate temperature field T^{**}.

(iii) Species corrector: Species equation at this stage is

$$\frac{\mathrm{d}}{\mathrm{d}t}(\rho Y_k) \approx Residual_s^*, \quad k = 1, \ldots, N \tag{27}$$

solution of which finalizes the first corrector stage yielding the second intermediate species field Y_k^{**}.

3.2.3. Second corrector stage

The second corrector stage is the same as first corrector stage except for the fact that all *Residual* expressions are computed at ** level. At the end of second corrector stage, third intermediate fields T^{***}, Y_k^{***} and $\mathbf{v}^{***}$ are obtained. This concludes the algorithm for one time step as the governing equations are now integrated from n to $n+1$ time level.

4. Numerical solution technique

In what follows, the components of the numerical solution technique will be explained in detail.

4.1. Computation of spatial derivatives using finite difference formulation

As discussed previously, the first stage of the MOL solution consists of discretization of the spatial derivatives which converts the system of PDEs into an ODE initial value problem. While evaluating the spatial derivatives, the convective terms should be approximated in such a way that the resulting system of ODEs is stable according to the linear stability theory [15]. In view of this, Oymak and Selçuk [19] used a five-point (fourth order) Lagrange interpolation polynomial based finite-difference discretization scheme which in its compact form can be written as follows

$$\frac{\partial u}{\partial x} = \sum_{i=1}^{5} b_i(x) u_i \tag{28}$$

where

$$b_i(x) = \frac{\sum_{\substack{k=1 \\ k\neq i}}^{5} \prod_{\substack{j=1 \\ j\neq i \\ j\neq k}}^{5} x - x_j}{\prod_{\substack{j=1 \\ j\neq i}}^{5} x_i - x_j} \tag{29}$$

Biased-upwind or biased-downwind stencils are chosen in a zone of dependence manner for the computation of convective terms and centered stencil is used for the diffusive terms which can be obtained by substituting $x = x_2$, $x = x_4$ and $x = x_3$ into Eq. (29), respectively. This approach was successfully applied to the MOL solution of diverse range of fluid flow problems [3,4,20].

In an attempt to apply the same principles to the simulation of chemically reacting flows, Tarhan [5] observed that spurious over- and under-shoots occur in the vicinity of the steep velocity and temperature gradients. The remedy proposed was the utilization of a second-order discretisation scheme based on Lagrange interpolation polynomials along with a Total Variation Diminishing (TVD) flux limiter. A numerical scheme is said to be TVD if the total variation does not increase in time. That is:

$$TV(u^{n+1}) \leqslant TV(u^n) \tag{30}$$

Here $TV(u^n)$ is the total variation of the numerical solution at the time level t^n which is defined as

$$TV(u^n) = \sum_i |u_{i+1} - u_i| \tag{31}$$

where u_i stands for the approximate solutions at mesh nodes x_i. Introducing Van Leer flux limiter [21] of the form

$$\Psi_i = \frac{r_i + |r_i|}{1 + |r_i|} \tag{32}$$

to second-order Lagrange interpolation based discretization scheme yields the following upwind and downwind expressions which satisfy the TVD condition, respectively:

$$\left.\frac{\partial u}{\partial x}\right|_i = \frac{u_i - u_{i-1}}{x_i - x_{i-1}} + \frac{1}{x_i - x_{i-2}}\left[\Psi_i(u_i - u_{i-1}) - \Psi_{i-1}\frac{x_i - x_{i-1}}{x_{i-1} - x_{i-2}}(u_{i-1} - u_{i-2})\right] \tag{33}$$

$$\left.\frac{\partial u}{\partial x}\right|_i = \frac{u_i - u_{i+1}}{x_i - x_{i+1}} + \frac{1}{x_i - x_{i+2}}\left[\Psi_i(u_i - u_{i+1}) - \Psi_{i+1}\frac{x_i - x_{i+1}}{x_{i+1} - x_{i+2}}(u_{i+1} - u_{i+2})\right] \tag{34}$$

The limiter Ψ_i is function of ratios of consecutive variations given by

$$r_i = \frac{(u_{i+1} - u_i)/(x_{i+1} - x_i)}{(u_i - u_{i-1})/(x_i - x_{i-1})} \tag{35}$$

for upwind scheme and

$$r_i = \frac{(u_{i-1} - u_i)/(x_{i-1} - x_i)}{(u_i - u_{i+1})/(x_i - x_{i+1})} \tag{36}$$

for downwind scheme, respectively.

In the present investigation, the diffusive and convective terms are discretized on non-staggered uniform grids using the schemes proposed by Oymak and Selçuk [19] and Tarhan [22], respectively.

4.2. Time integration

The most important feature of the MOL approach is that not only does it have the simplicity of the explicit methods but also the superiority of the implicit ones as higher-order implicit

time integration methods are employed in the solution of the resulting system of ODEs. There exist many efficient and reliable stiff ODE solvers in the open literature. However, it is very important to select a suitable solver considering the type and dimension of the physical system, desired level of accuracy and execution time. Based on the previous experience with a MOL based CFD code for the simulation of chemically reacting flows, implicit Adams–Moulton and BDF methods embedded in the state-of-the-art ODE solver LSODES [23] will be employed for time integration.

LSODES solves stiff and non-stiff systems of the form $\mathrm{d}y/\mathrm{d}t = f$. Non-stiff systems are handled by Adams methods (predictor-corrector) whereas BDF (GEAR methods) are used for the stiff cases. It determines the sparsity structure on its own (or optionally accepts this information from the user) and then uses parts of the Yale Sparse Matrix Package (YSMP) to solve the linear systems that arise, by a sparse (direct) LU factorization/backsolve method. LSODES supersedes, and improves upon, the older and well known GEARS package.

4.3. Numerical solution of the pressure equation

It has been shown that the present algorithm necessitates the solution of a elliptic pressure equation (also known as the pressure Poisson equation) at each momentum corrector stage. Utilization of classical iterative methods for the solution of pressure Poisson equation in time-dependent computations is computationally expensive and takes most of the computing effort. Direct or multigrid methods on the other hand are more attractive for these type of calculations owing to their efficiency and robustness [24]. Under the light of these facts, the present algorithm was equipped with a hybrid multigrid/direct solver namely MUDPACK [25]. MUDPACK is a collection of FORTRAN subprograms for the solution of linear elliptic PDEs which can operate on any bounded rectangular domain (not restricted to Cartesian coordinates) with any combination of boundary conditions. The second-order accurate results produced by the solver can be improved to fourth-order accuracy with ease using the method of deffered corrections.

For the solution of pressure equation of the form:

$$\nabla \cdot \nabla p^* = \mathit{Residual}_p^* \tag{37}$$

where

$$\mathit{Residual}_p^* \approx -\frac{1}{\Delta t}\left[(\nabla \cdot \rho^* \mathbf{v}^{**}) - (\nabla \cdot \rho^n \mathbf{v}^*)\right] - \nabla \cdot [\nabla \cdot \rho^n \mathbf{v}^* \mathbf{v}^*] - \nabla \cdot [\nabla \cdot \boldsymbol{\tau}^*] + \nabla \cdot \rho^n g \tag{38}$$

MUDPACK requires that the value of the $\mathit{Residual}_p^*$ term at each grid point is specified. For this purpose equation of continuity (Eq. (20)) is invoked which yields the following expression:

$$\mathit{Residual}_p^* \approx -\frac{1}{\Delta t}\left[\frac{(\rho^* - \rho^n)}{\Delta t} - (\nabla \cdot \rho^n \mathbf{v}^*)\right] - \nabla \cdot [\nabla \cdot \rho^n \mathbf{v}^* \mathbf{v}^*] - \nabla \cdot [\nabla \cdot \boldsymbol{\tau}^*] + \nabla \cdot \rho^n g \tag{39}$$

Due to the time-advanced density term (ρ^*) present in the right-hand side, Eq. (39) is implicit in time and hence cannot be directly used for the calculation of $\mathit{Residual}_p^*$ term. The generic procedure for eliminating the time-advanced density in favor of time-advanced pressure (p^*) is by using equation of state (Eq. (24)) which relates these two variables to one another. However, this in overall, results in a variable coefficient Poisson equation for pressure, solution of which is subject to stability problems [26]. Instead, a different approach is adopted in the present study: Considering the fact that the density variation in low Mach number flows is mostly due to temperature and concentration rather than pressure [13] and the former two remain unchanged during a momentum corrector stage, the first term in brackets in Eq. (39) is dropped yielding:

$$\mathit{Residual}_p^* \approx \frac{1}{\Delta t}(\nabla \cdot \rho^n \mathbf{v}^*) - \nabla \cdot [\nabla \cdot \rho^n \mathbf{v}^* \mathbf{v}^*] - \nabla \cdot [\nabla \cdot \boldsymbol{\tau}^*] + \nabla \cdot \rho^n g \tag{40}$$

In an attempt to verify the validity of the approach adopted, magnitudes of the first and second terms of Eq. (39) was compared. The analysis revealed that the former is three orders of magnitude smaller than the latter which fortifies the utilization of Eq. (40) for the computation of $\mathit{Residual}_p^*$ term.

Specification of boundary conditions is flexible in MUDPACK; use of any combination of periodic, Dirichlet and mixed-derivative boundary conditions is possible. In the present study, Dirichlet type boundary condition ($p = p_{\mathrm{ref}}$) was employed for outflow and derivative boundary conditions obtained from momentum equations of the form:

$$\nabla p = -[\nabla \cdot \rho \mathbf{v}\mathbf{v}] - [\nabla \cdot \boldsymbol{\tau}] + \rho g \tag{41}$$

were utilized for inflow, centerline and wall. The package and detailed documentation on the solvers can be obtained from [27].

4.4. Computation of radiative source term

For the computation of radiative source term, use has been made of a radiation code based on MOL solution of Discrete Ordinates Method (DOM) which was previously developed and applied to the simulation of steady-state radiative transfer in 2D axisymmetric, absorbing, emitting gray media [16], by means of coupling it to the CFD code.

The coupling strategy is mainly based on regular transfer of temperatures and concentrations solved by the CFD code to the radiation code which in turn provides source term field as the solution propagates in time. Owing to the nature of radiation transport, radiative heat transfer computations can be performed on much coarser grid resolutions when compared to that required for CFD. Hence rather than using identical grid resolutions for both CFD and radiation codes, two different resolutions were utilized: a fine mesh for CFD code and a coarse one enabling economic computation of radiative source term. Temperature and concentrations at the overlapping grid points of the coarse and fine meshes are transferred to the radiation code which calculates radiative source term for the CFD code. Source terms on the coarse mesh are redistributed to fine CFD

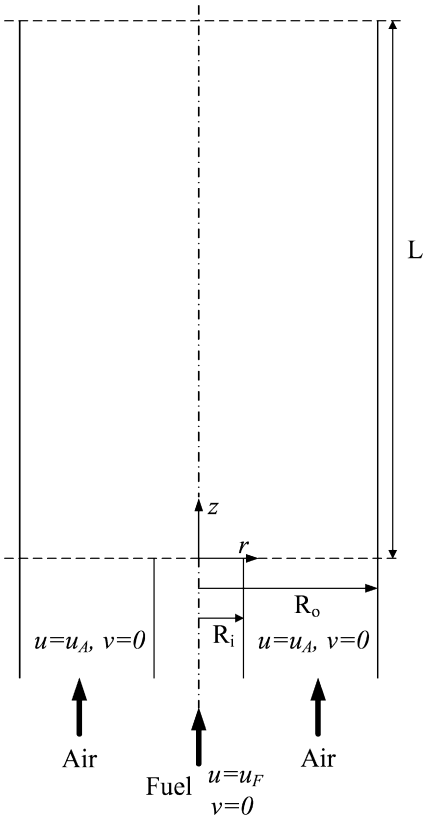

Geometrical Parameters:

R_i = 0.635 cm
R_o = 2.54 cm
L = 30 cm

Operating conditions:

Pressure at the exit of the burner: p = 1 atm
Wall temperature: T_w = 298 K

Inlet streams:

i) Inner tube (Fuel side):
Inflow axial velocity: u_F = 4.5 cm/s
Inflow radial velocity: v_F = 0.0 cm/s
Temperature: T_F = 298 K
Composition: Y_{CH_4} = 1.0

ii) Outer tube (Oxidizer side):
Inflow axial velocity: u_A = 9.88 cm/s
Inflow radial velocity: v_A = 0.0 cm/s
Temperature: T_A = 298 K
Composition: Y_{O_2} = 0.232, Y_{N_2} = 0.768

Fig. 2. Schematic diagram of confined axisymmetric laminar diffusion flame burner.

mesh via 2D interpolation. This cyclic loop is continued until steady-state which is dictated by the CFD code. Details regarding to the radiation code and coupling procedure can be found elsewhere [6,20].

4.5. Final remarks

So far, a non-iterative pressure based scheme for the solution of conservation equations of momentum, energy and species together with the numerical solution technique was presented. The formulations were given in vector notation for the sake of generality but the algorithm is equally applicable to any coordinate system. For the simulation of the problem under consideration, the algorithm was implemented in two-dimensional axisymmetric cylindrical coordinates. The singularities associated with the cylindrical coordinate system were surmounted using L'Hopital's rule where appropriate.

One other remark will be made on the selected grid topology. Most of the time, staggered grids are employed in pressure based schemes in order to avoid a phenomenon called odd-even decoupling or checker-board effect which can be described as the spurious pressure fluctuations occurring at the adjacent grid nodes. Despite the non-staggered grids utilized in the formulation, the possibility of a checker-board effect on the results was surmounted by the inclusion of density variation in the continuity equation for compressible flows as suggested by [28] together with the higher-order spatial discretization scheme employed in the computations.

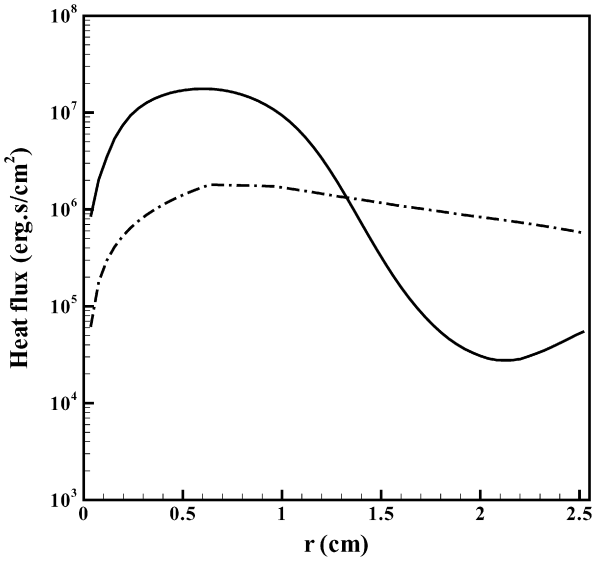

Fig. 3. Conductive and radiative heat fluxes in r-direction at the tip of the flame. ——— : Conduction; —·—·— : Radiation.

5. Results

For the evaluation of the performance of the algorithm for reacting radiating flows, use has been made of an atmospheric, axisymmetric, laminar methane-air diffusion flame (Fig. 2) previously studied by [5,7,8,29]. As initial conditions, the burner was assumed to be filled with stationary air at room temperature. The boundary conditions used in the solution of conser-

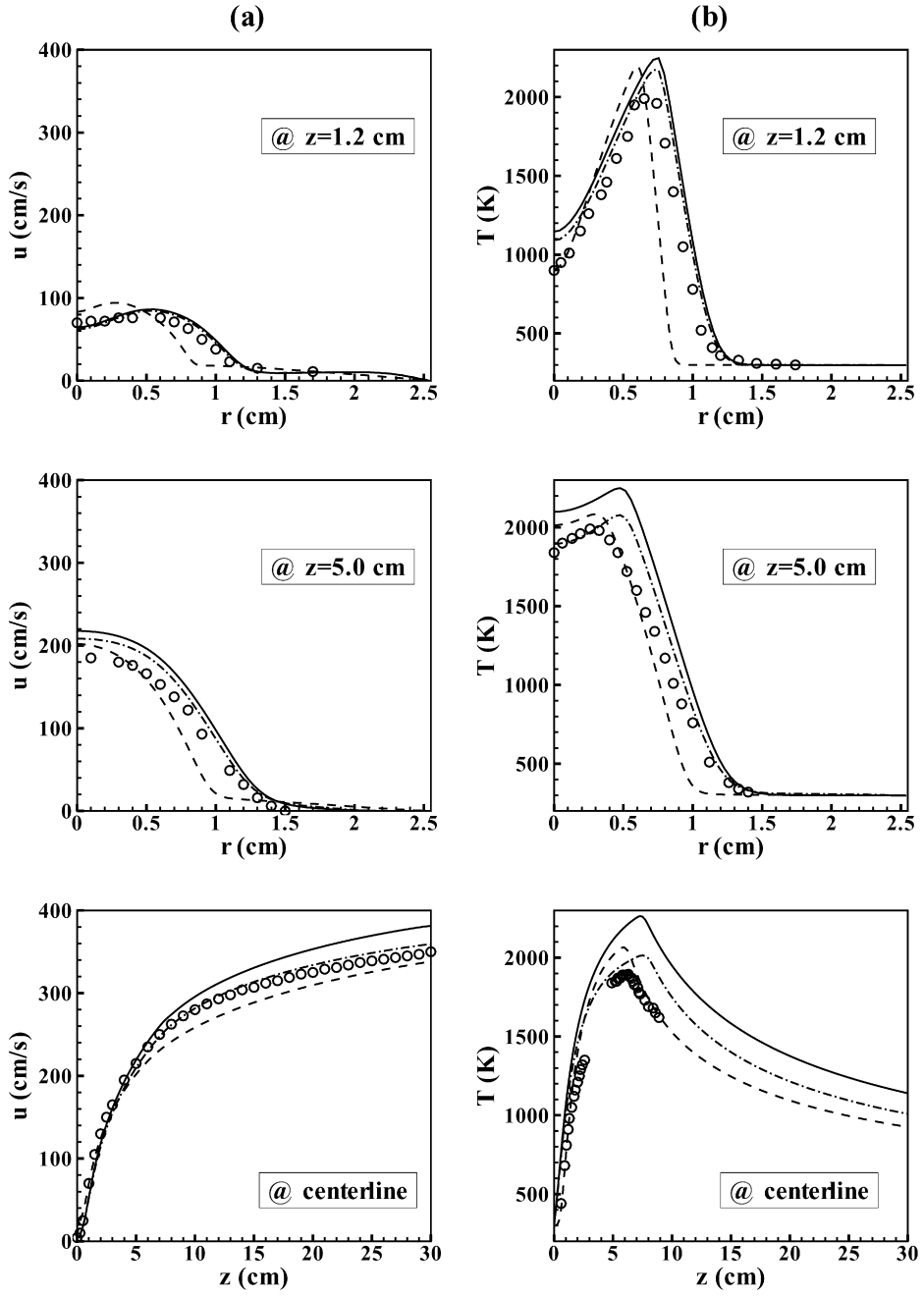

Fig. 4. Radial and axial profiles of axial velocity and temperature at two axial locations and along centerline: (a) Axial velocity; (b) Temperature. Symbol: Experiment [29]; - - - - : Predictions by Uygur et al. [6]; ——— : Present study (without radiation); — · — · — : Present study (with radiation).

vation equations were no-slip and no through-flow at the wall, symmetry along the centerline and developed conditions at the outflow, respectively. For radiative heat transfer calculations, all boundaries were assumed to be black with emissivities equal to unity. The flame was ignited by providing a local high temperature region ($T = 1500$ K) at the intersection of fuel and oxidizer streams for a time period of 50 ms.

The grid resolution requirement was determined by executing the algorithm for two different sets of grid resolutions: 65×129 for CFD and 9×17 for radiation (set 1); 65×161 for CFD and 9×21 for radiation (set 2); where in each pair the first and second numbers correspond to the number of grid points in r- and z-directions, respectively. It was seen that almost identical results were obtained with both sets and hence the coarser set (set 1) was selected as the grid resolution to be employed in CFD and radiation codes for CPU efficient simulations.

In order to determine the time step to be used for stable time-dependent calculations, executions with different time steps for the above-mentioned grid resolutions were performed. Upon testing, it was seen that stiffness brought by the chemical reactions can only be overcome with $\Delta t = 1 \times 10^{-5}$ s and further decreasing the time step (beyond $\Delta t = 1 \times 10^{-6}$ s) over-amplifies the $Residual_p$ term in the pressure Poisson equation (Eq. (37)) hence leading to unstable solutions. Therefore,

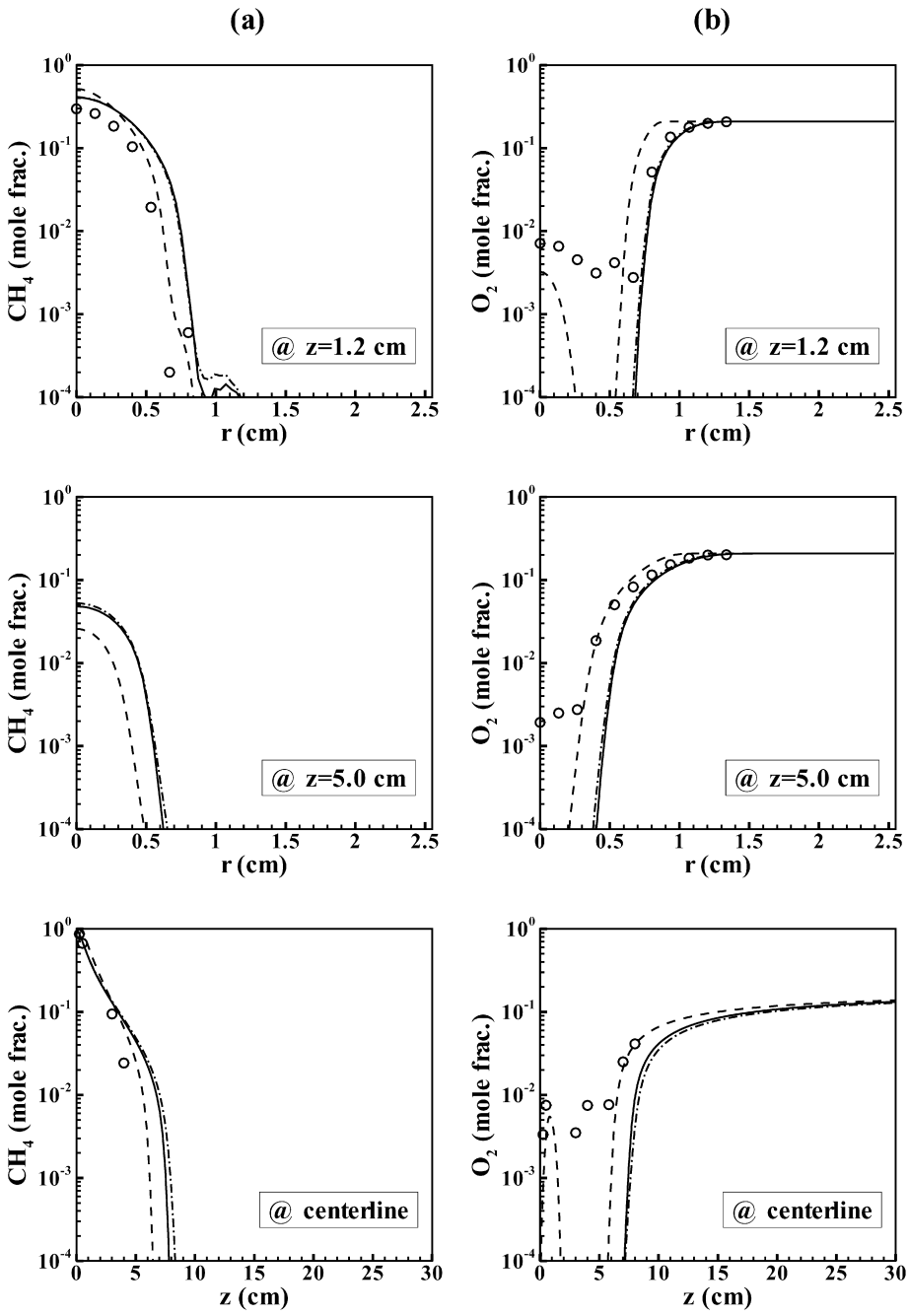

Fig. 5. Radial and axial profiles of CH_4 and O_2 mole fractions at two axial locations and along centerline: (a) CH_4; (b) O_2. Symbol: Experiment [29]; - - - - : Predictions by Uygur et al. [6]; ——— : Present study (without radiation); — · — · — : Present study (with radiation).

$\Delta t = 1 \times 10^{-5}$ s was designated as the time step to be employed in the calculations.

The computations were carried out on a Pentium IV 3.0 GHz PC having 2 GB of RAM. Numerical experimentation with two (one predictor, one corrector) and three stage (one predictor, two correctors) schemes revealed that the three stage scheme does not bring any improvement in accuracy and increases the computational effort significantly. Hence the results presented in this paper are produced with the two-stage scheme which took approximately 25 and 20 hours of CPU time for simulations with and without radiation, respectively.

The predictions of the algorithm were benchmarked against both experimental measurements [8] and numerical solutions [6] available on the test case. Figs. 4–6 illustrate the steady state axial velocity, temperature and species profiles with and without radiation. The reader should be informed at this stage that since the objective of this study is to present a new algorithm for the computation of reacting radiating flows, the discussions that follow will be based on the predictive performance of the algorithm with and without radiation rather than the flame characteristics.

Velocity and temperature profiles at two axial locations and along the centerline are displayed in Fig. 4. As can be seen,

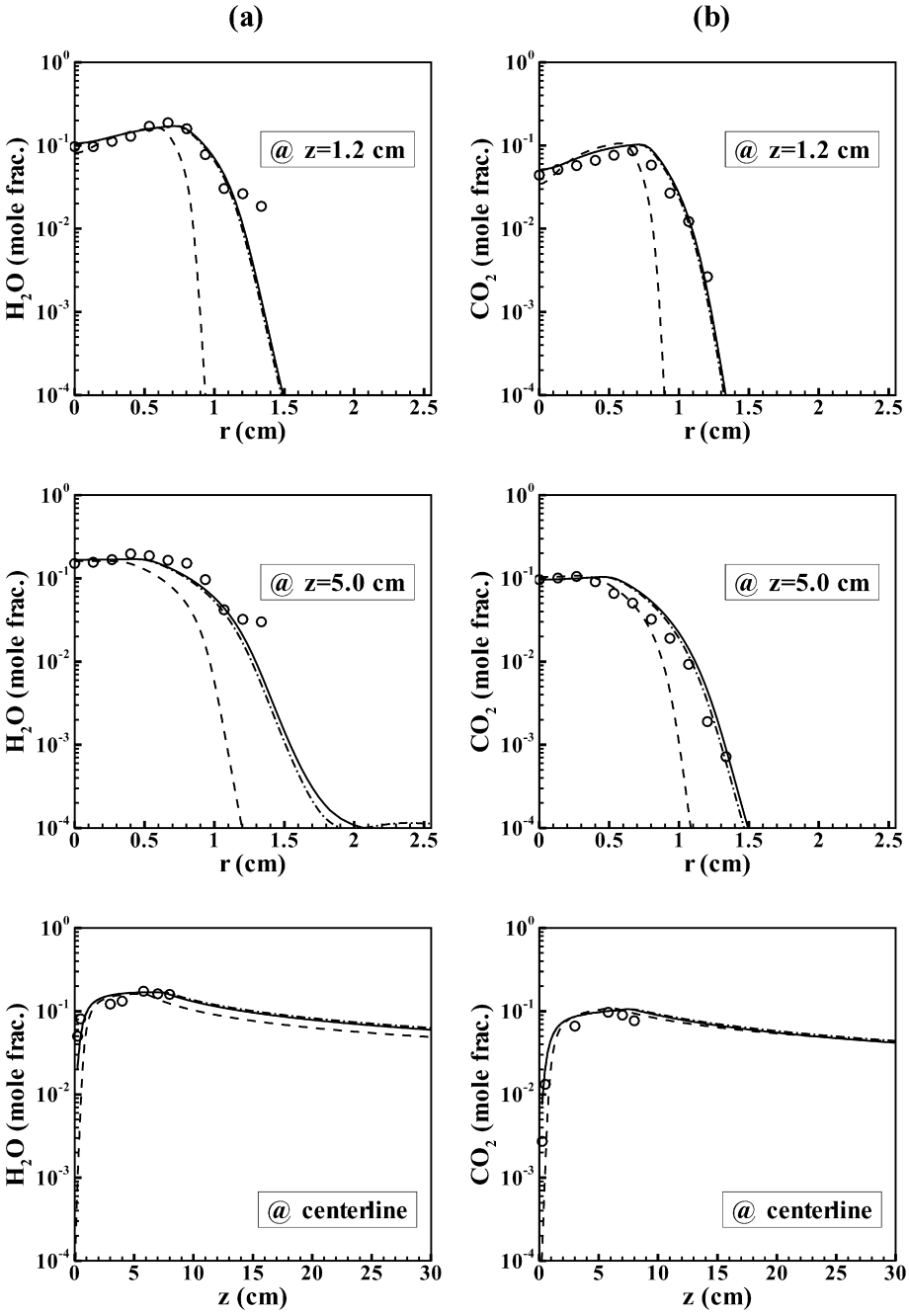

Fig. 6. Radial and axial profiles of H_2O and CO_2 mole fractions at two axial locations and along centerline: (a) H_2O; (b) CO_2. Symbol: Experiment [29]; - - - - : Predictions by Uygur et al. [6]; ——— : Present study (without radiation); — · — · — : Present study (with radiation).

predictions with and without radiation agree well with the experimental data at the first axial location and no significant discrepancy can be observed. However, the effect of incorporation of radiation is visualized better as downstream locations are reached where temperature and velocity profiles follow the experimental trends closer when compared to the predictions without radiation. In particular, peak temperature prediction displays favorable agreement with the experimental value. This is attributed to radiative heat losses which tend to decrease temperatures and in turn velocities.

The fuel and oxidizer profiles are shown in Fig. 5. As depicted by the figure, methane and oxygen profiles obtained by simulations with and without radiation are in reasonable agreement with the experimental measurements due to the simplicity of the reaction mechanism employed in the computations. A similar behavior was also observed by Tarhan [5] when the problem under consideration was simulated using one-step reaction mechanism and it was reported that utilization of multi-step reaction mechanism significantly improves the results in terms of agreement with the measurements.

Species profiles such as water-vapor and carbon-dioxide which are important in terms of radiative heat transfer are illustrated in Fig. 6. The figure shows that predictions with and

without radiation mimic the experimental data almost exactly. This finding places further confidence in radiative heat transfer computations since the concentrations of H_2O and CO_2 plays a crucial role in the calculation of absorption coefficients and hence radiative source terms which are used in the energy equation.

The performance of the present algorithm relative to the formerly developed code [6] was also assessed in terms of CPU time requirement to obtain steady state results and predictive accuracy, on the test case under consideration. Comparisons reveal that not only the CPU time requirement of the present code was approximately three times less than that required by [6] but a better accuracy was achieved as depicted by Figs. 4–6.

In an attempt to demonstrate the relative significance of radiative heat transfer with respect to transfer by conduction, radial profiles of radiative and conductive heat fluxes in r-direction at the tip of the flame ($z \approx 7.4$ cm) are plotted in Fig. 3. As can be seen from the figure, inside the flame, conduction is the superior mode of heat transfer owing to high temperature gradients occurring at this region whereas radiation is approximately ten times the transfer by conduction outside the flame. This behavior is consistent with the numerical results of Zhang [30] on the problem under consideration.

6. Conclusions

In what preceded, a non-iterative pressure based algorithm which consists of splitting the solution of momentum energy and species equations into a sequence of predictor–corrector stages was presented. The predictive performance of the algorithm was demonstrated on a typical methane/air diffusion flame. A global (one step) reaction mechanism was employed in the computations in order to account for the chemistry. Radiation calculations were carried out using a previously developed radiation code. The numerical results obtained with and without radiation were benchmarked against experimental and numerical measurements available in the literature. On the basis of numerical experimentation, it is concluded that:

- Despite the simplicity of the reaction mechanism employed in the computations, steady state velocity, temperature and major species concentration profiles obtained with and without radiation are overall in good agreement with the experimental data,
- Incorporation of radiation transport in the simulations has significant effect on the velocity and temperature fields and the agreement with the experimental data is better when compared to the computations without radiation,
- Utilization of more than one corrector stage does not bring any improvement in the accuracy and increases the computational effort significantly.

As a whole, the algorithm developed was proved to be an efficient and accurate tool for the simulation of reacting radiating flows and its extension to turbulent flows with the improvement of the existing models is highly promising.

References

[1] C.R. Kaplan, S.W. Baek, E.S. Oran, J.L. Ellzey, Dynamics of a strongly radiating unsteady ethylene jet diffusion flame, Combust. Flame 96 (1994) 1–21.

[2] O. Oymak, Method of lines solution of time-dependent 2D Navier–Stokes equations for incompressible separated flows, PhD thesis, Middle East Technical University, Turkey, 1997.

[3] T. Tarhan, N. Selçuk, Method of lines for transient flow fields, Int. J. Comput. Fluid Dynamics 15 (2001) 309–328.

[4] A.B. Uygur, T. Tarhan, N. Selçuk, MOL solution for transient turbulent flow in a heated pipe, Int. J. Thermal Sci. 44 (2004) 726–734.

[5] T. Tarhan, Numerical simulation of laminar reacting flows, PhD thesis, Middle East Technical University, Turkey, 2004.

[6] A.B. Uygur, T. Tarhan, N. Selçuk, Transient simulation of reacting radiating flows, Int. J. Thermal Sci. 45 (10) (2006) 969–976.

[7] Y. Xu, M.D. Smooke, Application of primitive variable Newton's method for the calculation of axisymmetric laminar diffusion flame, J. Comp. Phys. 109 (1993) 99–109.

[8] R.E. Mitchell, Nitrogen oxide formation in laminar methane–air diffusion flames, PhD thesis, MIT, 1975.

[9] O. Oymak, N. Selçuk, Method of lines solution of time-dependent two-dimensional Navier–Stokes equations, Int. J. Numer. Meth. Fluids 23 (5) (1996) 455–466.

[10] R.C. Martineau, An efficient semi-implicit pressure based scheme employing a high resolution finite element method for simulating transient and steady, inviscid and viscous, compressible flows on unstructured grids, PhD thesis, University of Idaho, USA, 2002.

[11] S.V. Patankar, D.B. Spalding, A calculation procedure for heat, mass and momentum transfer in three-dimensional parabolic flows, Int. J. Heat Mass Transfer 75 (1972) 1787–1806.

[12] R.I. Issa, Solution of the implicitly discretised fluid flow equations by operator splitting, J. Comp. Phys. 62 (1985) 40–65.

[13] R.I. Issa, B. Ahamadi-Befrui, K.R. Beshay, A.D. Gosman, Solution of implicitly discretized reacting flow equations by operator-splitting, J. Comp. Phys. 93 (1991) 388–410.

[14] E.E. Khalil, J.B. Spalding, J.H. Whitelaw, The calculation of local flow properties in two-dimensional furnaces, Int. J. Heat Mass Transfer 18 (1975) 775–791.

[15] W.E. Schiesser, The Numerical Method of Lines: Integration of Partial Differential Equations, Academic Press, New York, 1991.

[16] S. Harmandar, N. Selçuk, The method of line solution of discrete ordinated method for radiative heat transfer in cylindrical enclosures, J. Quant. Spectrosc. Radiat. Transfer 84 (4) (2004) 409–422.

[17] R.J. Kee, F.M. Rupley, E. Meeks, J.A. Miller, Chemkin-iii: A Fortran chemical kinetics package for the analysis of gas phase chemical and plasma kinetics, Sandia Laboratories, SAND96-8216, 1996.

[18] R.J. Kee, G. Dixon-Lewis, J. Warnatz, M.E. Coltrin, J.A. Miller, A Fortran computer code package for the evaluation of gas-phase, multicomponent transport properties, Sandia Laboratories, SAND86-8646, 1986.

[19] O. Oymak, N. Selcuk, Transient simulation of internal separated flows using an intelligent higher-order spatial discretization scheme, Int. J. Numer. Meth. Fluids 24 (1997) 759–769.

[20] N. Selçuk, A.B. Uygur, I. Ayranci, T. Tarhan, Transient simulation of radiating flows, J. Quant. Spectrosc. Radiat. Transfer 93 (3) (2005) 151–161.

[21] R.J. LeVeque, Numerical Methods for Conservation Laws, Birkhäuser-Verlag, Basel, 1992.

[22] T. Tarhan, N. Selçuk, Investigation of difference schemes on method of lines, Progress in Computational Fluid Dynamics, in press.

[23] K. Radhakrishnan, A.C. Hindmarsh, Description and use of LSODE, the Livermore solver for ordinary differential equations, Technical report, Lawrence Livermore National Laboratory, NASA, 1993.

[24] P. Wesseling, Principles of Computational Fluid Dynamics, Springer-Verlag, Berlin/New York, 2001.

[25] J.C. Adams, MUDPACK: Multigrid portable Fortran software for the efficient solution of linear elliptic partial differential equations, Appl. Math. Comput. 34 (1989) 113–146.

[26] B. Lessani, M.V. Papalexandris, Time-accurate calculation of variable density flows with strong temperature gradients and combustion, J. Comp. Phys. 212 (2006) 218–246.
[27] http://www.cisl.ucar.edu/css/software/mudpack/.
[28] J.D. Anderson, Computational Fluid Dynamics. The Basics with Applications, McGraw-Hill, New York, 1995.
[29] R.E. Mitchell, A.F. Sarofim, L.A. Clomburg, Experimental and numerical investigation of confined laminar diffusion flames, Combust. Flame 37 (1980) 227–244.
[30] Z. Zhang, Theoretical and computational study of coupling of soot, gas kinetics and radiation in diffusion flames using reduced mechanisms, PhD thesis, The University of Texas at Austin, 1998.